Formation and annealing of cubic ice: I. Modelling of stacking faults

2008 J. Phys.: Condens. Matter 20 285104

(http://iopscience.iop.org/0953-8984/20/28/285104)

J. Phys.: Condens. Matter **20** (2008) 285104 (12pp) doi:10.1088/0953-8984/20/28/285104

Formation and annealing of cubic ice: I. Modelling of stacking faults

T C Hansen[1], M M Koza[1] and W F Kuhs[2]

[1] Institut Laue-Langevin, 6 rue Jules Horowitz, BP 156, 38042 Grenoble Cedex, France
[2] Geowissenschaftliches Zentrum der Universität Göttingen, Abteilung Kristallographie, Goldschmidtstraße 1, 37077 Göttingen, Germany

E-mail: hansen@ill.fr

Received 8 January 2008, in final form 22 April 2008
Published 13 June 2008
Online at stacks.iop.org/JPhysCM/20/285104

Abstract

Ice Ic, so-called 'cubic ice' (König 1943 *Z. Kristallogr.* **105** 279–86), can be obtained, for example, from direct vapour deposition at low temperatures or by warming of recovered high-pressure forms of ice. It is usually obtained in the form of very small crystallites, leading to particle size broadening of the diffraction pattern. This pattern also contains features incompatible with a well-crystallized cubic structure, the details of which depend on the parent phase and the prevailing temperature. We have now corroborated an earlier suggestion (Kuhs *et al* 1987 *J. Physique* C1 **48** 631–6) that an important number of so-called deformation stacking faults exist in cubic ice and propose a model for a quantitative description of stacking faults and anisotropic particle size broadening in ice Ic suitable for profile refinements of its complex diffraction patterns.

(Some figures in this article are in colour only in the electronic version)

1. Introduction

Ice Ic, so-called 'cubic ice' [1], is the only crystalline form of ice formed at ambient pressure beside hexagonal, ice Ih, and its ordered low-temperature form, ice XI. It is usually obtained in the form of very small crystallites, e.g. by direct condensation from water vapour [1, 3–5] or by relaxation of recovered high-pressure phases of ice upon warming at ambient pressure [6–8].

It is frequently encountered in the temperature range from about 150 K to well over 200 K at ambient pressure. Unfortunately, none of the obtained ice Ic forms [4, 5, 9–12] shows the diffraction pattern one would expect from well-crystallized simple cubic ice, impeding any routine diffraction analysis of this material e.g. by means of Rietveld-type profile analysis of the diffraction data. It should be noted that the deviations from this idealized structure are different, depending on the starting material [1–6, 9–13]. Frequently, 'impurities' of ice Ih have been suggested as an explanation, e.g. [4, 5]. Arnold *et al* [11] realized that the diffraction peaks of cubic ice were substantially broadened. A closer peak shape investigation of the main cubic reflections and the appearance of broad peaks at Bragg angles typical for ice Ih lead to the assignment of the underlying defects as stacking faults [2]. The skewness of the cubic 111 and 222 reflections (shoulder at high or low angle, respectively) indicates qualitatively the presence of so-called deformation faults in contrast to so-called growth faults [14]. The first diffraction peak at low 2θ angle cannot be indexed assuming a cubic symmetry and corresponds to the 100 peak of hexagonal ice Ih. Its presence and the absence of further hexagonal reflections cannot be explained by a high concentration of growth faults but with either the existence of thin hexagonal sequences or by the occurrence of regular stacking sequences (polytypes) [2]. Elarby-Aouizerat *et al* have explained the high-angle shoulder of the 100 peak in terms of randomly oriented sheets of the ice Ih structure [12]. Crystallites of ice Ic are usually quite small. Considering isotropic spherical particles, the evaluation of the observed Bragg peaks according to the Scherrer formula leads to a diameter of 160 Å for ice Ic particles as from the relaxation of ice II [2], similar to the value of 130 Å found in [11]. Londono [15], based on high-resolution neutron data [16], reports 215 Å at 100 K and 384 Å at 176 K.

In a previous paper [17] we presented a way to fit the diffraction peak profiles with different models of stacking disorder [18]. This allows us to distinguish different samples with different histories in terms of their stacking distributions. An adapted range of sufficiently large unit cells with different, non-random stacking sequences is created for each sample and a linear combination of these replicas is fitted to the measured neutron diffraction data. In this

way a quantitative determination of the total amount of ice present can be obtained. However, this procedure is extremely time-consuming, as a very large number of long polytypes needs to be constructed, their diffraction patterns computed and combined. A refinement of the weighting factors of such a linear combination is virtually impossible, let alone the desirable refinement of other parameters such as lattice constants, Debye–Waller factors, anisotropic size broadening and atom positions. Alternatively we created with a Monte Carlo approach a best fitting polytype with a large number of layers to represent any form of ice Ic. However, such a polytype cannot be considered as a unique model to describe the bulk sample. Again, a refinement of any further parameter is hardly possible.

Therefore we proceed here with a semi-analytical approach close to the one used by Berliner and Werner [19], which described successfully the structure of stacking-faulted lithium metal. Due to the smallness of ice Ic crystallites, particle size broadening will need to be included in the modelling effort. The model will then be applied to diffraction data on the formation and annealing of ice Ic as described in the accompanying paper [20].

2. Experimental details

The structural model for ice Ic developed below was applied to neutron diffraction data of ice Ic obtained from recovered ice V and IX on the high-flux diffractometer D20 at the high-flux reactor of the Institut Laue-Langevin. Details of the sample preparation and data collection are given in the accompanying paper [20]. Figure 1 gives an appreciation of the changes of the first diffraction peaks as cubic ice is stepwise warmed up to a final temperature of 250 K. In agreement with earlier work, the reflections are substantially broadened at lower temperature with additional intensity on the shoulders and in between. A simple particle size broadened cubic ice (space group $Fd\bar{3}m$) cannot describe these intensities. It was suggested earlier [2] that stacking faults may well account for these additional intensities. Thus we turn now to possible ways of describing stacking faults in cubic ice.

3. Structure model

3.1. Scattering of stacking-faulted crystals

Crystals with stacking faults exhibit long-range order in two dimensions (the basal planes containing the primitive lattice translation vectors $\vec{a}$ and $\vec{b}$) but disorder amongst the basal planes along the third direction $\vec{c}$. If the crystal is taken to be of size $N_a \times N_b$ unit cells in transverse directions and N_c unit cells along the $\vec{c}$ direction, we get for a macroscopic crystal, for which N_a and N_b are large, the following differential scattering cross section:

$$\frac{\mathrm{d}\sigma(\vec{Q})}{\mathrm{d}\Omega} = \left| N_a N_b \delta(h-h_0)\delta(k-k_0) \times \sum_{m_3=-N_c}^{N_c} (N_c - |m_3|) Y_{m_3}(\vec{Q})\, \mathrm{e}^{2\pi \mathrm{i} m_3 l} \right|. \quad (1)$$

The function (1), as developed by Berliner and Werner [19], corresponds to the result obtained first by Wilson [21] and discussed by Guinier [22], and it also covers the 'Arten-und Lagenfehlordnung' discussed by Jagodzinski [23] as well as the 'variable phase' disorder considered by Hendricks and Teller [24].

The average structure factor product $Y_{m_3}(\vec{Q})$ determines the distribution of scattered intensity as a function of l along the nodal lines $(h_0 k_0)$. In the equation (2), $P_{\mathrm{A}_i \cdot \mathrm{A}_j}(m_3)$ corresponds to the probability of finding a layer A_j separated by a distance $m_3 \cdot c$ from a layer A_i. For N different types of layers from A_0 to A_N we have:

$$Y_{m_3}(\vec{Q}) = \frac{1}{N_c - |m_3|} \sum_{n=1}^{N_c-|m_3|} F_n F^*_{n+m_3} = \frac{1}{N_c - |m_3|} \sum_{n=1}^{N_c-|m_3|} \sum_{i=0}^{N} \sum_{j=0}^{N} P_{\mathrm{A}_i \cdot \mathrm{A}_j}(m_3) \cdot F_{\mathrm{A}_i} F^*_{\mathrm{A}_j}. \quad (2)$$

3.2. Stacking sequences—ABC notation

In the following, a fault is defined as a break in the sequence of alternation of close packed layers. A growth fault in a cubic close packed lattice (fcc) is the introduction of one hexagonal sequence: a sequence ABCABCABCAB becomes ABCAB<u>A</u>**CBACB**, the whole layer sequence is mirrored from the faulty plane onwards. A deformation fault corresponds to the formation of two adjacent hexagonal packing sequences: The layer sequence becomes ABCAB<u>AB</u>**CABC**. Starting from a hexagonal close packed lattice (hcp) a growth fault corresponds to the formation of one cubic packing sequence: ABABABAB becomes AB<u>C</u>**BCBCB** (structures of second type [18]). A deformation fault corresponds to the introduction of two (structures of third type: AB<u>CA</u>**CACA**) or three cubic packing sequences (structures of first type: AB<u>CAB</u>**ABA**). In all cases, more complex types of faults can be defined.

Now we need to define the different layers in ice Ic and ice Ih. In contrast to the simple metal considered by Berliner and Werner [19] we do not have mono-atomic hexagonal layers A, B and C. Nevertheless, it is common to define layers A, B and C in ice Ih and Ic in a way that allows us to apply the terminology of stacking faults as used for close packed metals. As one layer we regard the two one-fold oxygen atom positions, which lie in a lattice of hexagonal metric (subgroup $P3m1$ of space group $P6_3/mmc$, in which ice Ih crystallizes) on the same fractional x and y coordinates, but at different z ($\pm z$ above and below the layer's central plane perpendicular to $\vec{c}$), as shown in figure 2 for the example of the $9R$-polytype, a hypothetical structure between ideal ice Ic and Ih, which will be introduced in section 3.3 in more detail. The layers are indicated above the structure plot by the letters B C B C A .... The $\vec{c}$-axis is oriented horizontally. There are three different pairs (xy) possible: (00), $(\frac{1}{3}\frac{2}{3})$ and $(\frac{2}{3}\frac{1}{3})$. The fractional heights z in a hypothetical one-layer cell (half the height of the ice Ih cell in the direction of the $\vec{c}$ axis) are—idealized for the purely cubic case—$\frac{1}{8}$ and $\frac{7}{8}$ respectively. We have thus three equivalent layers A, B and C—if only oxygen is regarded. With the presence of hydrogen (or deuterium), a layer's content

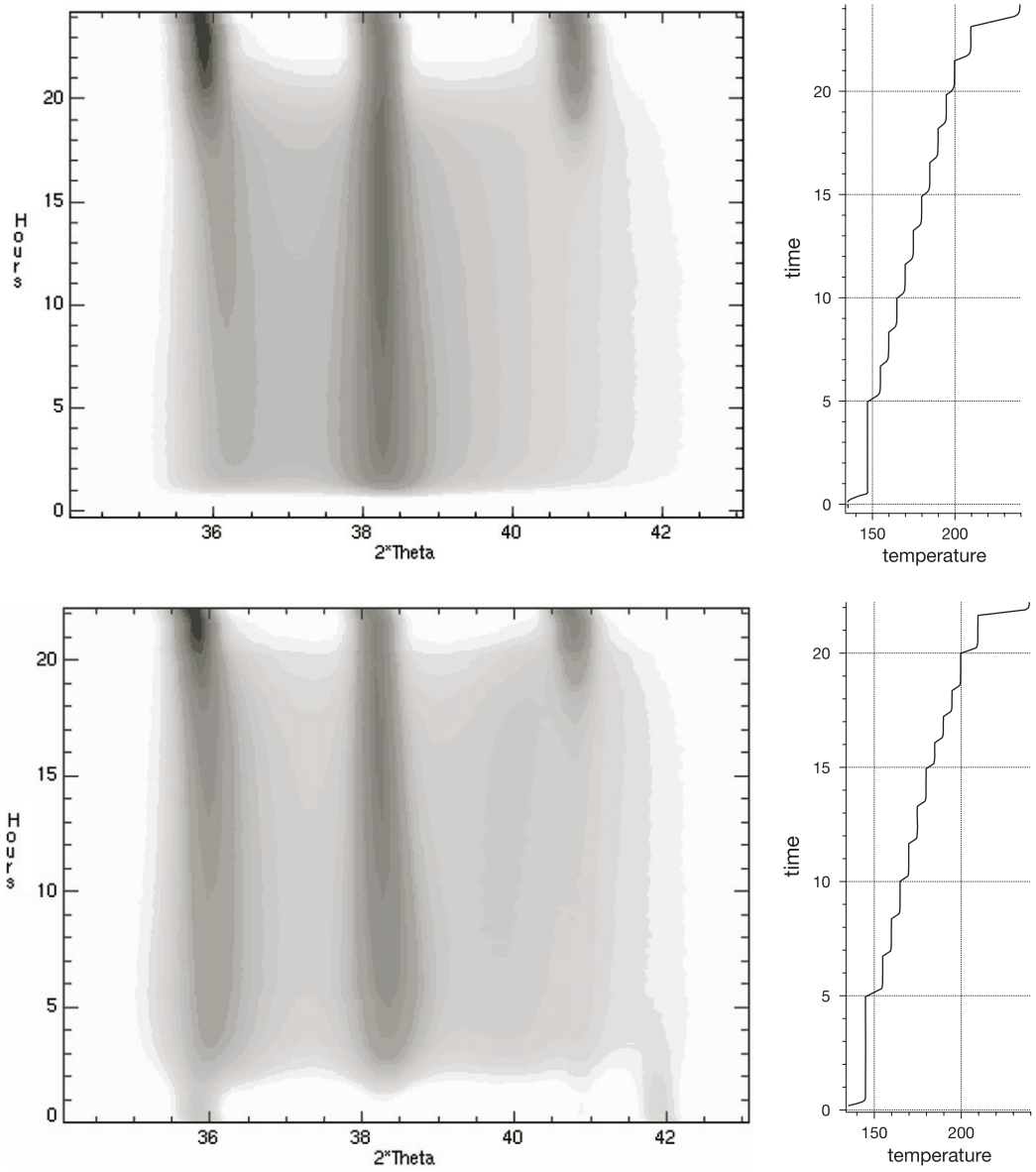

Figure 1. Logarithmic contour plot of powder diffraction intensity during formation and decomposition of ice Ic from ice V (top) and ice IX (bottom) precursors. Intensities are encoded from white (lowest) to black (highest). In the 2θ range shown (horizontal axis), one observes at the end of the run (top) from left to right the Bragg peaks 100, 002 and 101 of ice Ih. The 111 peak of ice Ic in the centre corresponds to the 002 peak of ice Ih. At the right side of each contour plot, the corresponding temperature profile of each diffraction series (time versus temperature) is plotted at the same timescale (vertical axis). Clearly visible is a sharpening of the 100_{hex} and 111_{cub} (002_{hex}) peak on temperature increase as well as the appearance of 101_{hex} above about 180 K. The intrinsic resolution of the instrument may be appreciated from the well-defined reflections of ice Ih finally formed above 240 K.

(and thus its structure factor) depends on its neighbours. There are four different 'versions' of a layer A: ${}_{\mathrm{C}}\mathrm{A}^{\mathrm{B}}$, ${}_{\mathrm{C}}\mathrm{A}^{\mathrm{C}}$, ${}_{\mathrm{B}}\mathrm{A}^{\mathrm{C}}$ and ${}_{\mathrm{B}}\mathrm{A}^{\mathrm{B}}$, and in total we have to deal with 12 different layers, which would result in $12^2 = 144$ correlated interference terms in the sum of the average structure factor product defined in equation (2).

The further treatment of a confusingly high number of terms can be significantly reduced by a different layer definition: compared to the previous definition, the border of a layer is only shifted by half a one-layer unit cell. Now the centre plane of a layer is at $z = 0$ instead of $z = \frac{1}{2}$, and the two oxygen positions of a layer are closer to this centre plane ($z = -\frac{1}{8}$ and $z = +\frac{1}{8}$ in the ideal cubic case) but have necessarily different fractional coordinates x and y. We shall call these layers after the previous definition AB, BC, CA, BA, AC and CB. The layers correspond, thus, to the interfaces between the previously presented, 'conventionally' defined layers. There are only six different layers possible, resulting in $6^2 = 36$ correlated terms in (2). An ideal cubic sequence ('3C') would be $[\mathrm{AB{\cdot}BC{\cdot}CA{\cdot}}]_\infty$, with $[\mathrm{BA{\cdot}AC{\cdot}CB{\cdot}}]_\infty$ being perfectly equivalent. A perfectly hexagonal sequence ('2H') would be $[\mathrm{AB{\cdot}BA{\cdot}}]_\infty$, with $[\mathrm{BC\cdot CB{\cdot}}]_\infty$ and $[\mathrm{CA{\cdot}AC{\cdot}}]_\infty$ being perfectly equivalent. Note, that perfectly hexagonal sequences contain a mirror-plane between two layers.

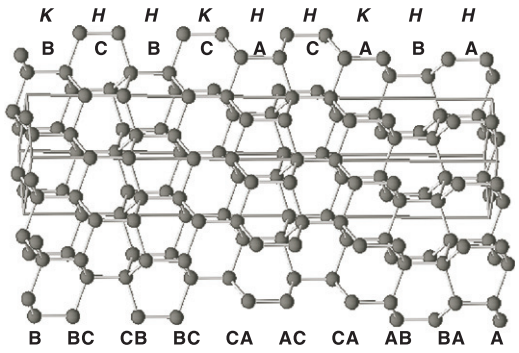

Figure 2. Structure model of hypothetical *hhc*-ice (9*R*); only the oxygen positions are shown. The $\vec{c}$-axis runs horizontally. The top row of letters gives the HK notation (see section 3.3) for the displayed stacking sequences denoting the local character of the stacking as cubic ('K') or hexagonal ('H'): a K-sequence is characterized by a local inversion centre relating the neighbouring puckered layers and sitting in the centre of the hydrogen-bond joining the layers along the *c*-axis, an H-sequence is characterized by a local mirror-plane (NB: both, inversion centre and mirror-plane, consider only the idealized oxygen positions). The second row of letters (A, B, C) denotes the three possible locations of the joining hydrogen-bond connecting the puckered layers along the *c*-axis. The bottom row of letters gives the interface layer notation and represents the possible arrangements of the puckered double layers in terms of the three possible oxygen positions in the *ab*-plane. The relation between the different notations is further elucidated in figure 3.

With this definition, (2) can be rewritten with 36 interference terms in the sum:

$$\begin{aligned}
Y_{m_3}(\vec{Q}) = {} & P_{\mathrm{AB\cdot AB}}(m_3)F_{\mathrm{AB}}F^*_{\mathrm{AB}} + P_{\mathrm{AB\cdot BC}}(m_3)F_{\mathrm{AB}}F^*_{\mathrm{BC}} \\
& + P_{\mathrm{AB\cdot CA}}(m_3)F_{\mathrm{AB}}F^*_{\mathrm{CA}} + P_{\mathrm{AB\cdot BA}}(m_3)F_{\mathrm{AB}}F^*_{\mathrm{BA}} \\
& + P_{\mathrm{AB\cdot CB}}(m_3)F_{\mathrm{AB}}F^*_{\mathrm{CB}} + P_{\mathrm{AB\cdot AC}}(m_3)F_{\mathrm{AB}}F^*_{\mathrm{AC}} \\
& + P_{\mathrm{BC\cdot AB}}(m_3)F_{\mathrm{BC}}F^*_{\mathrm{AB}} + P_{\mathrm{BC\cdot BC}}(m_3)F_{\mathrm{BC}}F^*_{\mathrm{BC}} \\
& + P_{\mathrm{BC\cdot CA}}(m_3)F_{\mathrm{BC}}F^*_{\mathrm{CA}} + P_{\mathrm{BC\cdot BA}}(m_3)F_{\mathrm{BC}}F^*_{\mathrm{BA}} \\
& + P_{\mathrm{BC\cdot CB}}(m_3)F_{\mathrm{BC}}F^*_{\mathrm{CB}} + P_{\mathrm{BC\cdot AC}}(m_3)F_{\mathrm{BC}}F^*_{\mathrm{AC}} \\
& + P_{\mathrm{CA\cdot AB}}(m_3)F_{\mathrm{CA}}F^*_{\mathrm{AB}} + P_{\mathrm{CA\cdot BC}}(m_3)F_{\mathrm{CA}}F^*_{\mathrm{BC}} \\
& + P_{\mathrm{CA\cdot CA}}(m_3)F_{\mathrm{CA}}F^*_{\mathrm{CA}} + P_{\mathrm{CA\cdot BA}}(m_3)F_{\mathrm{CA}}F^*_{\mathrm{BA}} \\
& + P_{\mathrm{CA\cdot CB}}(m_3)F_{\mathrm{CA}}F^*_{\mathrm{CB}} + P_{\mathrm{CA\cdot AC}}(m_3)F_{\mathrm{CA}}F^*_{\mathrm{AC}} \\
& + P_{\mathrm{BA\cdot AB}}(m_3)F_{\mathrm{BA}}F^*_{\mathrm{AB}} + P_{\mathrm{BA\cdot BC}}(m_3)F_{\mathrm{BA}}F^*_{\mathrm{BC}} \\
& + P_{\mathrm{BA\cdot CA}}(m_3)F_{\mathrm{BA}}F^*_{\mathrm{CA}} + P_{\mathrm{BA\cdot BA}}(m_3)F_{\mathrm{BA}}F^*_{\mathrm{BA}} \\
& + P_{\mathrm{BA\cdot CB}}(m_3)F_{\mathrm{BA}}F^*_{\mathrm{CB}} + P_{\mathrm{BA\cdot AC}}(m_3)F_{\mathrm{BA}}F^*_{\mathrm{AC}} \\
& + P_{\mathrm{AC\cdot AB}}(m_3)F_{\mathrm{AC}}F^*_{\mathrm{AB}} + P_{\mathrm{AC\cdot BC}}(m_3)F_{\mathrm{AC}}F^*_{\mathrm{BC}} \\
& + P_{\mathrm{AC\cdot CA}}(m_3)F_{\mathrm{AC}}F^*_{\mathrm{CA}} + P_{\mathrm{AC\cdot BA}}(m_3)F_{\mathrm{AC}}F^*_{\mathrm{BA}} \\
& + P_{\mathrm{AC\cdot CB}}(m_3)F_{\mathrm{AC}}F^*_{\mathrm{CB}} + P_{\mathrm{AC\cdot AC}}(m_3)F_{\mathrm{AC}}F^*_{\mathrm{AC}} \\
& + P_{\mathrm{CB\cdot AB}}(m_3)F_{\mathrm{CB}}F^*_{\mathrm{AB}} + P_{\mathrm{CB\cdot BC}}(m_3)F_{\mathrm{CB}}F^*_{\mathrm{BC}} \\
& + P_{\mathrm{CB\cdot CA}}(m_3)F_{\mathrm{CB}}F^*_{\mathrm{CA}} + P_{\mathrm{CB\cdot BA}}(m_3)F_{\mathrm{CB}}F^*_{\mathrm{BA}} \\
& + P_{\mathrm{CB\cdot CB}}(m_3)F_{\mathrm{CB}}F^*_{\mathrm{CB}} + P_{\mathrm{CB\cdot AC}}(m_3)F_{\mathrm{CB}}F^*_{\mathrm{AC}}. \qquad (3)
\end{aligned}$$

Here, $P_{\mathrm{AB\cdot AB}}(m_3)$ is the probability of finding two AB-layers separated by a distance m_3c, $P_{\mathrm{AB\cdot BC}}(m_3)$ the probability of finding a layer BC separated by m_3c from a layer AB, and so on. In order to specify the arrangement of layers, we only require four probabilities, $P_{\mathrm{AB\cdot AB}}(m_3)$, $P_{\mathrm{AB\cdot BA}}(m_3)$, $P_{\mathrm{AB\cdot BC}}(m_3)$ and $P_{\mathrm{AB\cdot CA}}(m_3)$. As the identification of a given layer in a macroscopic sample as A, B or C is purely arbitrary, the pairs AB–AB, BC–BC, CA–CA, AC–AC, CB–CB and BA–BA are equally probable, thus, the total probability of finding two identical double layers out of six at a distance of m_3c can be expressed by $P_{\mathrm{AB\cdot AB}}(m_3)$. Equally, the six pairs AB–BA, BC–CB, CA–AC, AC–CA, CB–BC and BA–AB are equivalent and thus their probability is $P_{\mathrm{AB\cdot BA}}(m_3)$. For $P_{\mathrm{AB\cdot AB}}(m_3)$ and $P_{\mathrm{AB\cdot BA}}(m_3)$ inversion of the sign of m_3 results in the same probability. Note, that only these two probabilities have values different from zero in a perfect hexagonal stacking sequence, which is the only one containing mirror planes perpendicular to $\vec{c}$. This is not the case for the probabilities $P_{\mathrm{AB\cdot BC}}(m_3)$ and $P_{\mathrm{AB\cdot CA}}(m_3)$, corresponding again to the probability of finding one of six pairs at a distance of m_3c: here we have the relation $P_{\mathrm{AB\cdot CA}}(m_3) = P_{\mathrm{AB\cdot BC}}(-m_3)$. These probabilities become non-zero only if cubic stacking sequences occur. The probability of having one of the remaining 12 possible pairs occurring is simply $P_{\mathrm{AB\cdot AC}}(m_3) = 1 - P_{\mathrm{AB\cdot AB}}(m_3) - P_{\mathrm{AB\cdot BA}}(m_3) - P_{\mathrm{AB\cdot BC}}(m_3) - P_{\mathrm{AB\cdot CA}}(m_3)$. Note, that in the case of a simple close packed metal, as described by Berliner and Werner in [19], not only does the equation equivalent to (3) contain nine terms, but also the probabilities condense down to only one probability $p(m_3)$ that two layers separated by a distance m_3c are identical instead of the four different probabilities presented above. Thus, equation (3) can be rewritten simplified but will remain far more complex than for a close packed metal:

$$\begin{aligned}
Y_{m_3}(\vec{Q}) = {} & \frac{P_{\mathrm{AB\cdot AB}}(m_3)}{6}F_{\mathrm{AB}}F^*_{\mathrm{AB}} + \frac{P_{\mathrm{AB\cdot BC}}(m_3)}{6}F_{\mathrm{AB}}F^*_{\mathrm{BC}} \\
& + \frac{P_{\mathrm{AB\cdot CA}}(m_3)}{6}F_{\mathrm{AB}}F^*_{\mathrm{CA}} + \frac{P_{\mathrm{AB\cdot BA}}(m_3)}{6}F_{\mathrm{AB}}F^*_{\mathrm{BA}} \\
& + \frac{P_{\mathrm{AB\cdot AC}}(m_3)}{12}F_{\mathrm{AB}}F^*_{\mathrm{CB}} + \frac{P_{\mathrm{AB\cdot AC}}(m_3)}{12}F_{\mathrm{AB}}F^*_{\mathrm{AC}} \\
& + \frac{P_{\mathrm{AB\cdot CA}}(m_3)}{6}F_{\mathrm{BC}}F^*_{\mathrm{AB}} + \frac{P_{\mathrm{AB\cdot AB}}(m_3)}{6}F_{\mathrm{BC}}F^*_{\mathrm{BC}} \\
& + \frac{P_{\mathrm{AB\cdot BC}}(m_3)}{6}F_{\mathrm{BC}}F^*_{\mathrm{CA}} + \frac{P_{\mathrm{AB\cdot AC}}(m_3)}{12}F_{\mathrm{BC}}F^*_{\mathrm{BA}} \\
& + \frac{P_{\mathrm{AB\cdot BA}}(m_3)}{6}F_{\mathrm{BC}}F^*_{\mathrm{CB}} + \frac{P_{\mathrm{AB\cdot AC}}(m_3)}{12}F_{\mathrm{BC}}F^*_{\mathrm{AC}} \\
& + \frac{P_{\mathrm{AB\cdot BC}}(m_3)}{6}F_{\mathrm{CA}}F^*_{\mathrm{AB}} + \frac{P_{\mathrm{AB\cdot CA}}(m_3)}{6}F_{\mathrm{CA}}F^*_{\mathrm{BC}} \\
& + \frac{P_{\mathrm{AB\cdot AB}}(m_3)}{6}F_{\mathrm{CA}}F^*_{\mathrm{CA}} + \frac{P_{\mathrm{AB\cdot AC}}(m_3)}{12}F_{\mathrm{CA}}F^*_{\mathrm{BA}} \\
& + \frac{P_{\mathrm{AB\cdot AC}}(m_3)}{12}F_{\mathrm{CA}}F^*_{\mathrm{CB}} + \frac{P_{\mathrm{AB\cdot BA}}(m_3)}{6}F_{\mathrm{CA}}F^*_{\mathrm{AC}} \\
& + \frac{P_{\mathrm{AB\cdot BA}}(m_3)}{6}F_{\mathrm{BA}}F^*_{\mathrm{AB}} + \frac{P_{\mathrm{AB\cdot AC}}(m_3)}{12}F_{\mathrm{BA}}F^*_{\mathrm{BC}} \\
& + \frac{P_{\mathrm{AB\cdot AC}}(m_3)}{12}F_{\mathrm{BA}}F^*_{\mathrm{CA}} + \frac{P_{\mathrm{AB\cdot AB}}(m_3)}{6}F_{\mathrm{BA}}F^*_{\mathrm{BA}} \\
& + \frac{P_{\mathrm{AB\cdot CA}}(m_3)}{6}F_{\mathrm{BA}}F^*_{\mathrm{CB}} + \frac{P_{\mathrm{AB\cdot BC}}(m_3)}{6}F_{\mathrm{BA}}F^*_{\mathrm{AC}} \\
& + \frac{P_{\mathrm{AB\cdot AC}}(m_3)}{12}F_{\mathrm{AC}}F^*_{\mathrm{AB}} + \frac{P_{\mathrm{AB\cdot AC}}(m_3)}{12}F_{\mathrm{AC}}F^*_{\mathrm{BC}} \\
& + \frac{P_{\mathrm{AB\cdot BA}}(m_3)}{6}F_{\mathrm{AC}}F^*_{\mathrm{CA}} + \frac{P_{\mathrm{AB\cdot CA}}(m_3)}{6}F_{\mathrm{AC}}F^*_{\mathrm{BA}} \\
& + \frac{P_{\mathrm{AB\cdot BC}}(m_3)}{6}F_{\mathrm{AC}}F^*_{\mathrm{CB}} + \frac{P_{\mathrm{AB\cdot AB}}(m_3)}{6}F_{\mathrm{AC}}F^*_{\mathrm{AC}}
\end{aligned}$$

$$+\frac{P_{\mathrm{AB\cdot AC}}(m_3)}{12}F_{\mathrm{CB}}F^*_{\mathrm{AB}}+\frac{P_{\mathrm{AB\cdot BA}}(m_3)}{6}F_{\mathrm{CB}}F^*_{\mathrm{BC}}$$
$$+\frac{P_{\mathrm{AB\cdot AC}}(m_3)}{12}F_{\mathrm{CB}}F^*_{\mathrm{CA}}+\frac{P_{\mathrm{AB\cdot BC}}(m_3)}{6}F_{\mathrm{CB}}F^*_{\mathrm{BA}}$$
$$+\frac{P_{\mathrm{AB\cdot AB}}(m_3)}{6}F_{\mathrm{CB}}F^*_{\mathrm{CB}}+\frac{P_{\mathrm{AB\cdot CA}}(m_3)}{6}F_{\mathrm{CB}}F^*_{\mathrm{AC}} \quad (4)$$

$$Y_{m_3}(\vec{Q})=\frac{P_{\mathrm{AB\cdot AB}}(m_3)}{6}\big(F_{\mathrm{AB}}F^*_{\mathrm{AB}}+F_{\mathrm{BC}}F^*_{\mathrm{BC}}+F_{\mathrm{CA}}F^*_{\mathrm{CA}}$$
$$+F_{\mathrm{BA}}F^*_{\mathrm{BA}}+F_{\mathrm{AC}}F^*_{\mathrm{AC}}+F_{\mathrm{CB}}F^*_{\mathrm{CB}}\big)+\frac{P_{\mathrm{AB\cdot BC}}(m_3)}{6}$$
$$\times\big(F_{\mathrm{AB}}F^*_{\mathrm{BC}}+F_{\mathrm{BC}}F^*_{\mathrm{CA}}+F_{\mathrm{CA}}F^*_{\mathrm{AB}}+F_{\mathrm{BA}}F^*_{\mathrm{AC}}$$
$$+F_{\mathrm{AC}}F^*_{\mathrm{CB}}+F_{\mathrm{CB}}F^*_{\mathrm{BA}}\big)+\frac{P_{\mathrm{AB\cdot CA}}(m_3)}{6}$$
$$\times\big(F_{\mathrm{AB}}F^*_{\mathrm{CA}}+F_{\mathrm{BC}}F^*_{\mathrm{AB}}+F_{\mathrm{CA}}F^*_{\mathrm{BC}}+F_{\mathrm{BA}}F^*_{\mathrm{CB}}$$
$$+F_{\mathrm{AC}}F^*_{\mathrm{BA}}+F_{\mathrm{CB}}F^*_{\mathrm{AC}}\big)+\frac{P_{\mathrm{AB\cdot BA}}(m_3)}{6}$$
$$\times\big(F_{\mathrm{AB}}F^*_{\mathrm{BA}}+F_{\mathrm{BC}}F^*_{\mathrm{CB}}+F_{\mathrm{CA}}F^*_{\mathrm{AC}}$$
$$+F_{\mathrm{BA}}F^*_{\mathrm{AB}}+F_{\mathrm{AC}}F^*_{\mathrm{CA}}+F_{\mathrm{CB}}F^*_{\mathrm{BC}}\big)$$
$$+\big\{1-P_{\mathrm{AB\cdot AB}}(m_3)-P_{\mathrm{AB\cdot BA}}(m_3)-P_{\mathrm{AB\cdot BC}}(m_3)$$
$$-P_{\mathrm{AB\cdot CA}}(m_3)\big\}\tfrac{1}{12}$$
$$\times\big(F_{\mathrm{AB}}F^*_{\mathrm{CB}}+F_{\mathrm{AB}}F^*_{\mathrm{AC}}+F_{\mathrm{BC}}F^*_{\mathrm{BA}}+F_{\mathrm{BC}}F^*_{\mathrm{AC}}$$
$$+F_{\mathrm{CA}}F^*_{\mathrm{BA}}+F_{\mathrm{CA}}F^*_{\mathrm{CB}}+F_{\mathrm{BA}}F^*_{\mathrm{BC}}+F_{\mathrm{BA}}F^*_{\mathrm{CA}}$$
$$+F_{\mathrm{AC}}F^*_{\mathrm{AB}}+F_{\mathrm{AC}}F^*_{\mathrm{BC}}+F_{\mathrm{CB}}F^*_{\mathrm{AB}}+F_{\mathrm{CB}}F^*_{\mathrm{CA}}\big). \quad (5)$$

For our purposes in this paper, we assume that the displacements of the lattice nodes due to the presence of stacking faults are negligible. We consider only two fractional position parameters: d, which is the deflection of the oxygen position out of the central plane of an interface layer in fractions of c, $\frac{1}{8}$ in the case of ideal cubic ice, and g, which is the relative position of one of the two half-occupied hydrogen positions on the connection line between two oxygen positions, about 0.36 in the case of hexagonal ice. This one parameter does not take into account properly the difference between the two different crystallographic positions of hydrogen in hexagonal ice or the fact that not all four oxygen–oxygen distances are the same, but it is a sufficiently precise approximation for the later refinement of medium resolution powder diffraction patterns. With this we have the following structure factors for the 10-atomic interface layers (two oxygen positions and eight half-occupied hydrogen positions):

$$F_{\mathrm{AB}}=\tfrac{1}{2}((((\mathrm{e}^{-\frac{2}{3}\mathrm{i}((g-1)h+2(g-1)k+3d(1-2g)l)\pi}$$
$$+\mathrm{e}^{-\frac{2}{3}\mathrm{i}((g-1)h-g+k+3d(1-2g)l)\pi}$$
$$+\mathrm{e}^{\frac{2}{3}\mathrm{i}((g+2)h-(g+2)k+3d(1-2g)l)\pi}$$
$$+\mathrm{e}^{\frac{2}{3}\mathrm{i}((g+2)h+2(g+2)k+3d(1-2g)l)\pi}$$
$$+\mathrm{e}^{\frac{2}{3}\mathrm{i}(2(g-1)h+(g-1)k+3d(2g-1)l)\pi}$$
$$+\mathrm{e}^{-\frac{2}{3}\mathrm{i}(2(g+2)h+(g+2)k+3d(2g-1)l)\pi}$$
$$+\mathrm{e}^{\frac{2}{3}\mathrm{i}(2h+k-3(2gd-d+g)l)\pi}$$
$$+\mathrm{e}^{\frac{2}{3}\mathrm{i}(h+2k+3(2gd-d+g)l)\pi}))b_{\mathrm{H}}+2((\mathrm{e}^{\frac{2}{3}\mathrm{i}(h+2k-3dl)\pi}$$
$$+\mathrm{e}^{\frac{2}{3}\mathrm{i}(2h+k+3dl)\pi}))b_{\mathrm{O}}))$$

$$F_{\mathrm{BC}}=\tfrac{1}{2}((((\mathrm{e}^{-2\mathrm{i}(2gd-d+g)l\pi}$$
$$+\mathrm{e}^{-\frac{2}{3}\mathrm{i}((g-2)h-(g-2)k+3d(1-2g)l)\pi}$$
$$+\mathrm{e}^{-\frac{2}{3}\mathrm{i}((g-2)h+2(g-2)k+3d(1-2g)l)\pi}$$
$$+\mathrm{e}^{\frac{2}{3}\mathrm{i}(2(g-2)h+(g-2)k+3d(2g-1)l)\pi}+\mathrm{e}^{\frac{2}{3}\mathrm{i}(2h+k+3(2gd-d+g)l)\pi}$$
$$+\mathrm{e}^{\frac{2}{3}\mathrm{i}(3dl+g(h-k-6dl))\pi}$$
$$+\mathrm{e}^{\frac{2}{3}\mathrm{i}(3dl+g(h+2k-6dl))\pi}$$
$$+\mathrm{e}^{-\frac{2}{3}\mathrm{i}(g(2h+k+6dl)-3dl)\pi}))b_{\mathrm{H}}$$
$$+2((\mathrm{e}^{2\mathrm{i}dl\pi}+\mathrm{e}^{\frac{2}{3}\mathrm{i}(2h+k-3dl)\pi}))b_{\mathrm{O}}))$$

$$F_{\mathrm{CA}}=\tfrac{1}{2}\mathrm{e}^{-2\mathrm{i}dl\pi}((((\mathrm{e}^{2\mathrm{i}(2d+1)gl\pi}+\mathrm{e}^{-\frac{2}{3}\mathrm{i}g(h+2k-6dl)\pi}$$
$$+\mathrm{e}^{\frac{2}{3}\mathrm{i}g(-h+k+6dl)\pi}+\mathrm{e}^{\frac{2}{3}\mathrm{i}g(2h+k+6dl)\pi}$$
$$+\mathrm{e}^{-\frac{2}{3}\mathrm{i}(-(g+1)h+(g+1)k+6d(g-1)l)\pi}$$
$$+\mathrm{e}^{-\frac{2}{3}\mathrm{i}(2(g+1)h+(g+1)k+6d(g-1)l)\pi}$$
$$+\mathrm{e}^{\frac{2}{3}\mathrm{i}(gh+h+2gk+2k+6dl-6dgl)\pi}$$
$$+\mathrm{e}^{\frac{2}{3}\mathrm{i}(h+2k-3(2d(g-1)+g)l)\pi}))b_{\mathrm{H}}$$
$$+2((1+\mathrm{e}^{\frac{2}{3}\mathrm{i}(h+2k+6dl)\pi}))b_{\mathrm{O}}))$$

$$F_{\mathrm{AC}}=\tfrac{1}{2}((((\mathrm{e}^{-2\mathrm{i}(2gd-d+g)l\pi}$$
$$+\mathrm{e}^{-\frac{2}{3}\mathrm{i}(2(g+1)h+gk+k+3dl-6dgl)\pi}$$
$$+\mathrm{e}^{\frac{2}{3}\mathrm{i}(gh+h-gk-k-3dl+6dgl)\pi}$$
$$+\mathrm{e}^{\frac{2}{3}\mathrm{i}(gh+h+2gk+2k-3dl+6dgl)\pi}$$
$$+\mathrm{e}^{\frac{2}{3}\mathrm{i}(h+2k+3(2gd-d+g)l)\pi}$$
$$+\mathrm{e}^{\frac{2}{3}\mathrm{i}(3dl+g(2h+k-6dl))\pi}$$
$$+\mathrm{e}^{-\frac{2}{3}\mathrm{i}(g(h-k+6dl)-3dl)\pi}$$
$$+\mathrm{e}^{-\frac{2}{3}\mathrm{i}(g(h+2k+6dl)-3dl)\pi}))b_{\mathrm{H}}$$
$$+2((\mathrm{e}^{2\mathrm{i}dl\pi}+\mathrm{e}^{\frac{2}{3}\mathrm{i}(h+2k-3dl)\pi}))b_{\mathrm{O}}))$$

$$F_{\mathrm{CB}}=\tfrac{1}{2}\mathrm{e}^{-2\mathrm{i}dl\pi}((((\mathrm{e}^{2\mathrm{i}(2d+1)gl\pi}+\mathrm{e}^{-\frac{2}{3}\mathrm{i}g(2h+k-6dl)\pi}$$
$$+\mathrm{e}^{\frac{2}{3}\mathrm{i}g(h-k+6dl)\pi}+\mathrm{e}^{\frac{2}{3}\mathrm{i}g(h+2k+6dl)\pi}$$
$$+\mathrm{e}^{\frac{2}{3}\mathrm{i}(2(g-2)h+(g-2)k-6d(g-1)l)\pi}$$
$$+\mathrm{e}^{-\frac{2}{3}\mathrm{i}((g-2)h-(g-2)k+6d(g-1)l)\pi}$$
$$+\mathrm{e}^{-\frac{2}{3}\mathrm{i}((g-2)h+2(g-2)k+6d(g-1)l)\pi}$$
$$+\mathrm{e}^{\frac{2}{3}\mathrm{i}(2h+k-3(2d(g-1)+g)l)\pi}))b_{\mathrm{H}}$$
$$+2((1+\mathrm{e}^{\frac{2}{3}\mathrm{i}(2h+k+6dl)\pi}))b_{\mathrm{O}}))$$

$$F_{\mathrm{BA}}=\tfrac{1}{2}((((\mathrm{e}^{\frac{2}{3}\mathrm{i}(2(g-1)h+(g-1)k+3d(1-2g)l)\pi}$$
$$+\mathrm{e}^{-\frac{2}{3}\mathrm{i}(2(g+2)h+(g+2)k+3d(1-2g)l)\pi}$$
$$+\mathrm{e}^{-\frac{2}{3}\mathrm{i}((g-1)h+2(g-1)k+3d(2g-1)l)\pi}$$
$$+\mathrm{e}^{-\frac{2}{3}\mathrm{i}((g-1)h-gk+k+3d(2g-1)l)\pi}$$
$$+\mathrm{e}^{\frac{2}{3}\mathrm{i}((g+2)h-(g+2)k+3d(2g-1)l)\pi}$$
$$+\mathrm{e}^{\frac{2}{3}\mathrm{i}((g+2)h+2(g+2)k+3d(2g-1)l)\pi}$$

$$+ e^{\frac{2}{3}i(h+2k-3(2gd-d+g)l)\pi}$$
$$+ e^{\frac{2}{3}i(2h+k+3(2gd-d+g)l)\pi}))b_H$$
$$+ 2((e^{\frac{2}{3}i(2h+k-3dl)\pi} + e^{\frac{2}{3}i(h+2k+3dl)\pi}))b_O)). \quad (6)$$

Here, in the case of neutron scattering, b_O and b_H are the nuclear scattering lengths of oxygen and hydrogen (or deuterium), respectively, which are independent of the scattering vector $\vec{Q}$. For x-ray diffraction, b_O and b_H would have to be replaced by the wavevector dependent atomic form factor $f(Q)$.

3.3. Polytypes—HK notation

The calculation of $P_{AB\cdot AB}(m_3)$, $P_{AB\cdot BA}(m_3)$, $P_{AB\cdot BC}(m_3)$ and $P_{AB\cdot CA}(m_3)$ requires a specification of the underlying stacking sequence. As we had reasons to suspect in [17] that ice Ic, formed from ice IX, is close to a $9R$-lattice (see figure 2), of which the prototype is samarium metal [25, 26], we shall elaborate this procedure here on this example. The $9R$ designation [27] specifies a nine-layer crystal with a rhombohedral space group. The stacking sequence for this structure can be represented by the A, B and C layer notation or by denoting each layer as H (hexagonal) or K (cubic) depending on its local environment [23]. Note, that sometimes the symbols h (hexagonal) and c (cubic) are used instead, so in [17] a layer that has two different layers adjacent on either side is denoted as a K layer, while a layer that has similar layers adjacent on either side is denoted as an H layer. The description of the $9R$ structure requires an interaction range of $s = 4$, e.g. no interaction between every fourth layer. Four independent probabilities α, β, γ and δ are needed for this interaction range [23], which represents the probability that two adjacent layers of type HH, HK, KH or KK respectively, are followed by a K layer. All polytypes with $S < 4$ can be defined with a set of these probabilities. The perfect $9R$ sequence corresponds to $\alpha = 1$, $\beta = 0$, $\gamma = 0$ and $\delta = 0$, a perfect cubic lattice would have $\alpha = 1$, $\beta = 1$, $\gamma = 1$ and $\delta = 1$, a hexagonal one $\alpha = 0$, $\beta = 0$, $\gamma = 0$ and $\delta = 0$. Isolated deformation faults in a cubic lattice correspond to the introduction of two adjacent H layers, while an isolated twin (or growth) fault produces a single H layer amongst a sequence of K layers. If we only consider these two faults at a probability of $P_{deformation}$ and P_{twin} in a cubic lattice, we have [19]:

$$\alpha = 1, \qquad \beta = 1, \qquad \gamma = \frac{P_{twin}}{P_{deformation} + P_{twin}} \quad (7)$$
$$\text{and} \qquad \delta = 1 - (P_{deformation} + P_{twin}).$$

We can now simulate faulted crystals as special cases of an $s = 4$ lattice. It is straightforward to 'grow' a crystal in the computer using the four probabilities α, β, γ and δ as defined above. However, we must introduce the concept of crystal 'seeds'. The beginning sequences of a computer simulation must be consistent with the choices of α, β, γ and δ. This self-consistent selection of seeds is obtained by consideration of the pair-occurrence probabilities w_{HH}, w_{HK}, w_{KH} and w_{KK}

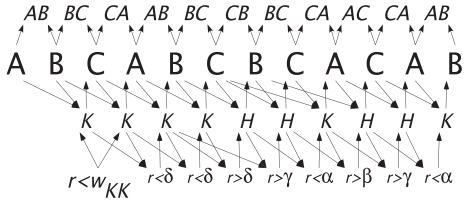

Figure 3. An example of a computer-grown stacking sequence resulting from a set of probabilities $\alpha = 63\%$, $\beta = 39\%$, $\gamma = 35\%$ and $\delta = 78\%$ and the output $0 < r < 1$ of a random number generator. The lowest row schematizes the probability tests, the following one the resulting stacking rules in HK notation, followed by the consequent layers in ABC notation and, in the top row, the interface layer notation introduced in section 3.2.

for HH, HK, KH and KK pairs, respectively [19]:

$$w_{HK} = \frac{\alpha(1-\delta)}{(1-\gamma)(1-\delta) + 2\alpha(1-\delta) + \alpha\beta}$$
$$w_{KH} = w_{HK}$$
$$w_{HH} = w_{HK}(1-\gamma) \quad (8)$$
$$w_{KK} = \frac{\beta w_{HK}}{1-\delta}.$$

Calculation of $P_{AB\cdot AB}(m_3)$, $P_{AB\cdot BA}(m_3)$, $P_{AB\cdot BC}(m_3)$ and $P_{AB\cdot CA}(m_3)$ is accomplished by growth of an N_c-layer crystallite N times in the computer using the random number generator. Growth of each crystallite begins with the first two layers as an A and a B layer. The following two layers correspond to one of the four possible seeds: HH corresponds to ABAB, HK to ABAC, KH to ABCB and KK to ABCA. The type of the next layer (H or K) is determined by comparing the random number generator output to the appropriate probability α, β, γ or δ. If the type is H, the next layer $m_3 + 1$, out of A, B or C, will be identical to the layer $m_3 - 1$, otherwise it will be different from m_3 and $m_3 - 1$. The computer has thus to keep track of the layers $m_3 - 1$ and m_3 and the layer type of the layers $m_3 - 2$ and $m_3 - 1$. This process is repeated until the N_c-layer crystallite is completed.

The growth of a crystal shall be shown on an example, which is demonstrated in figure 3. Let r be a random number in the range from 0 to 1. We assume $\alpha = 63\%$, $\beta = 39\%$, $\gamma = 35\%$ and $\delta = 78\%$, which is actually the real situation of figure 5, at the end of the 175 K stage of ice Ic from ice V. From this we get with (8) $w_{HH} = 21\%$. The random number generator delivers $r = 39\% > w_{HH} = 21\%$, which means that the first two stacking rules to apply are not HH. Again, from (8), we have $w_{KK} = 38\%$ or $w_{KK}/(1 - w_{KK}) = 48\%$. This time, the random number generator delivers $r = 45\% < w_{KK}/(1 - w_{KK}) = 48\%$, which means that the first two stacking rules to apply are KK. The third and fourth layer of the crystal are thus both packed obeying the cubic stacking rule: the new layer to add is not equal to the previous two. For the third layer, the previous layers being A and B, this results in C, for the fourth layer, the previous layers being B and C, this results in A. The sequence at this stage is ABCA so far. To find out, which stacking rule has to be applied to determine

the following layer, we note that the previously applied rules were K and K. Thus, we have to check the probability δ that two cubic stacking rules are followed by a cubic one. The random number generator delivers $r = 66\% < \delta = 78\%$, which means that again a cubic stacking rule has to be applied. The fifth layer, the previous ones being C and A thus becomes B, the crystal can be described as ABCAB so far. For the sixth layer we get $r = 2\% < \delta = 78\%$, again obeying the rule K, thus giving C and resulting in ABCABC. For the seventh layer we get $r = 86\% > \delta = 78\%$. This time a hexagonal stacking rule H follows the previous two rules K and K, the consequent layer has to be identical to the one preceding the previous layer and with the two preceding layers being B and C this results in a layer B. The whole stack becomes ABCABCB. The two previously applied stacking rules being K and H we have now to check the probability γ that a sequence of rules KH is followed by a rule K. The random number generator delivers $r = 37\% > \gamma = 35\%$, which means that a hexagonal stacking rule H has to be applied to generate the eighth layer. With the preceding layers CB this new layer becomes C and the whole stack ABCABCBC. With the two preceding stacking rules HH, the probability α that HH is followed by K has to be checked now. With $r = 12\% < \alpha = 63\%$ we have to apply the rule K and the ninth layer becomes different from the two preceding ones, BC, so is A. The whole stack now is described by ABCABCBCA. With the two preceding stacking rules HK, the probability β that HK is followed by K has to be checked next. With $r = 91\% > \beta = 39\%$ we have to apply the rule H and the tenth layer becomes, with preceding layers CA, C, so the whole stack is thus ABCABCBCAC. The two previously applied stacking rules being KH we have now to check the probability γ again and with $r = 79\% > \gamma = 35\%$ we have to apply H and generate a layer A. With the two preceding stacking rules HH, the probability α has to be checked now. With $r = 26\% < \alpha = 63\%$ we have to apply K and the twelfth layer becomes different from the two preceding ones, CA, so B. The whole stack is now ABCABCBCACAB. The stacking rules applied so far have been KKKKHHKHHK, which could be considered as two deformation faults in an otherwise purely cubic sequence. In terms of interface layers the same stack can be written as ABBCCAABBCCBBCCAACCAAB.

The quantity $P_{\mathrm{AB\cdot AB}}(m_3)$ is determined by analysing each one of the N crystallites: we compare layer pairs at a distance of m_3 and get the probability that these pairs are identical. For $P_{\mathrm{AB\cdot BA}}(m_3)$ the approach is similar, only that we do look out for pairs which contain identical layers but which are inverted. $P_{\mathrm{AB\cdot BC}}(m_3)$ and $P_{\mathrm{AB\cdot CA}}(m_3)$ are probabilities that these pairs contain only one identical layer either as far from each other or as close as possible. For each set of probabilities α, β, γ and δ we thus get a characteristic set of $P_{\mathrm{AB\cdot AB}}(m_3)$, $P_{\mathrm{AB\cdot BA}}(m_3)$, $P_{\mathrm{AB\cdot BC}}(m_3)$ and $P_{\mathrm{AB\cdot CA}}(m_3)$. We need to grow a certain number N of crystallites in order that these probabilities converge (except for pure polytypes like the perfectly cubic, the perfectly hexagonal and the $9R$ lattice). For the computing-intense refinements we have chosen $N = 500$ in contrast to Berliner and Werner [19] who have chosen $N = 10\,000$. But in contrast to them, we get a better 'counting statistics' on the probabilities as we evaluate all distances m_3 occurring

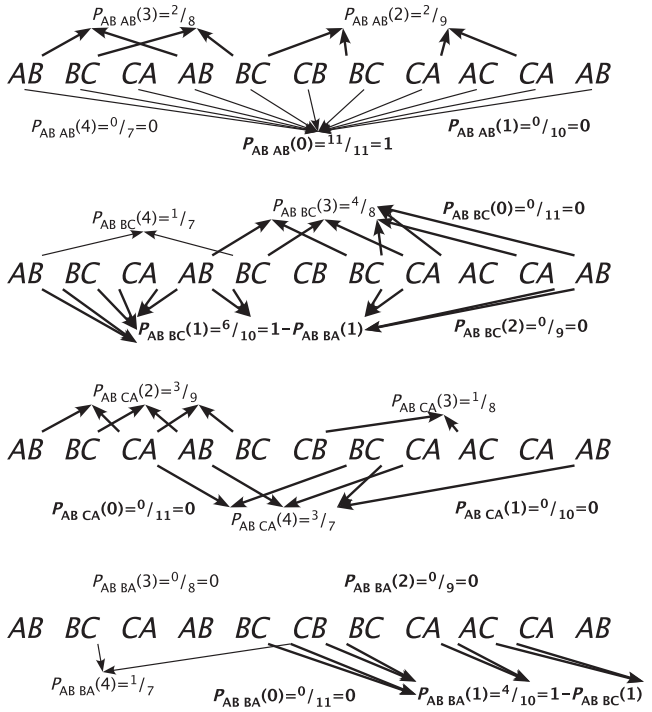

Figure 4. Example of a computer-grown stacking sequence from figure 3. The deduction of each of the four independent pair correlation probabilities for $m_3 = 0$–4 is shown, arrows indicate the contributing pairs, probabilities which have general values for all stacking sequences are printed in bold.

in a crystallite: in a crystallite with $N_c = 100$ we have, for example, $N_c - m_3 = 98$ correlating pairs with $m_3 = 2$ which we use to evaluate the probabilities $P_{\mathrm{AB\cdot AB}}(m_3)$, $P_{\mathrm{AB\cdot BA}}(m_3)$, $P_{\mathrm{AB\cdot BC}}(m_3)$ and $P_{\mathrm{AB\cdot CA}}(m_3)$, while Berliner and Werner only compare the first layer with the layer $m_3 + 1$ to determine the layer–layer correlation probabilities. This procedure gives a sufficient convergence for smaller values of m_3 and bad convergence for values of m_3 approaching N_c, but terms with a high value of m_3 have a very small influence on the result anyway, as seen from equation (1).

The counting of pair correlation probabilities shall be shown on the same example: $P_{\mathrm{AB\cdot AB}}(0)$ is always one (identity), $P_{\mathrm{AB\cdot AB}}(1)$ is always zero (the following interface layer must start with the same layer as the previous one ends), $P_{\mathrm{AB\cdot AB}}(2)$ is 2/9 in our example (from nine possible pairs separated by $m_3 = 2$ layers we find two identical ones, BC-BC and CA-CA), $P_{\mathrm{AB\cdot BA}}(0)$ is always zero, $P_{\mathrm{AB\cdot BA}}(1)$ is 4/10 in our example (from ten possible pairs separated by $m_3 = 1$ layers—thus direct neighbours—we find inverted pairs four times, BC–CB, CB–BC, CA–AC and AC–CA), $P_{\mathrm{AB\cdot BA}}(2)$ is always zero, because inverted layer pairs separated by two layers would imply a sandwiched interface pair in between which is type AA, BB or CC, which is not possible. Further counting of pair correlation probabilities is demonstrated in figure 4.

Some generalities are noteworthy: $P_{\mathrm{AB\cdot AB}}(0) = 1$, $P_{\mathrm{AB\cdot BA}}(0) = P_{\mathrm{AB\cdot BC}}(0) = P_{\mathrm{AB\cdot CA}}(0) = P_{\mathrm{AB\cdot AB}}(1) = P_{\mathrm{AB\cdot CA}}(1) = P_{\mathrm{AB\cdot BA}}(2) = P_{\mathrm{AB\cdot BC}}(2) = 0$ and $P_{\mathrm{AB\cdot BA}}(1) + P_{\mathrm{AB\cdot BC}}(1) = 1$. All four probabilities $P_{\mathrm{AB\cdot AB}}(m_3)$,

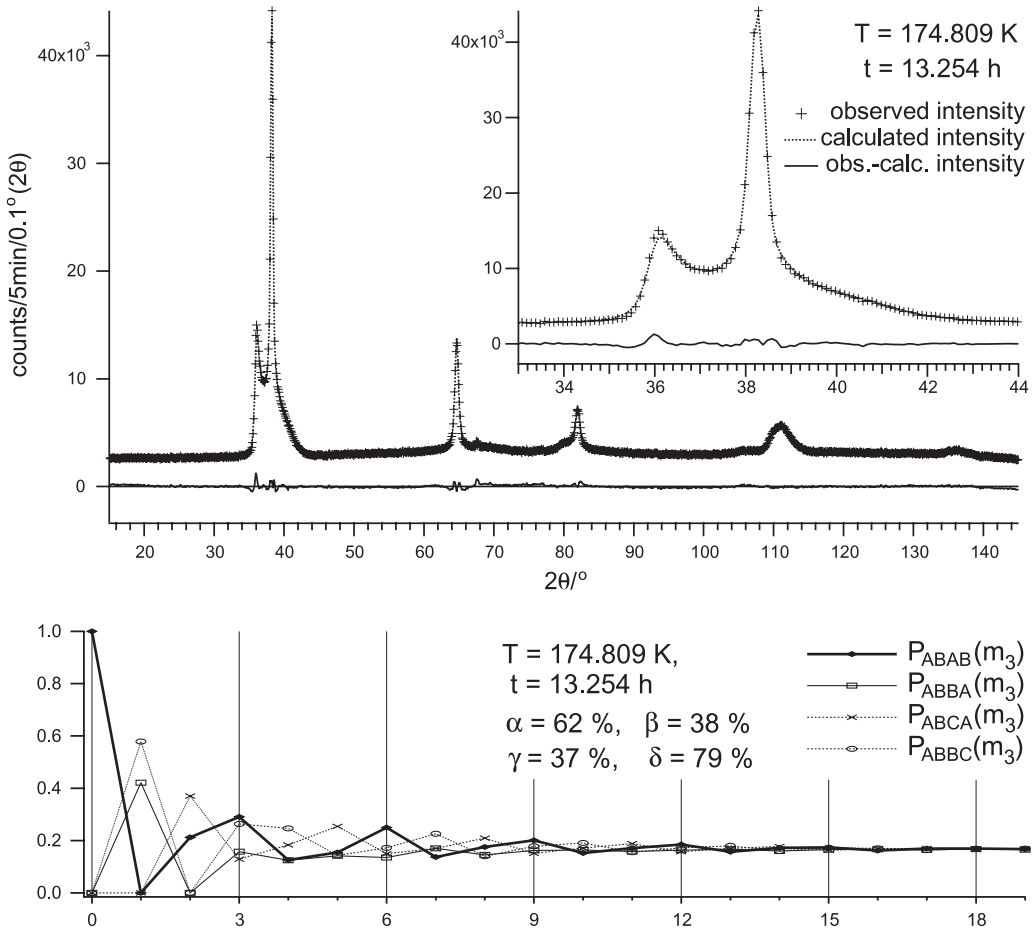

Figure 5. Diffraction pattern and fit of ice Ic from ice V at the end of the 175 K stage after 13.3 h (top) and pair correlation probabilities in ice Ic at these conditions (bottom).

$P_{\mathrm{AB{\cdot}BA}}(m_3)$, $P_{\mathrm{AB{\cdot}BC}}(m_3)$ and $P_{\mathrm{AB{\cdot}CA}}(m_3)$ approach 1/6 for large values of m_3 (if any stacking fault occurs, e.g. if α, β, γ and δ are not all equal to one or zero).

3.4. Algorithm for model refinement

The computing of powder patterns of stacking-faulted ice Ic/Ih has been set up in the commercial software *Igor Pro* [28]. The routine computing of the pair correlation probabilities has been set up partially using a so-called *XOP* [29], an external module entirely programmed in C, which accelerates this part by a factor of 50. The routine builds N times a stacking sequence of N_c layers based upon the set of probabilities α, β, γ or δ and starting from the self-consistent set of 'seeds'. The *XOP* extracts from these sequences $P_{\mathrm{AB{\cdot}AB}}(m_3)$, $P_{\mathrm{AB{\cdot}BA}}(m_3)$, $P_{\mathrm{AB{\cdot}BC}}(m_3)$ and $P_{\mathrm{AB{\cdot}CA}}(m_3)$.

Another *XOP* computes the scattered intensity as a function of l (about 10 times faster than an *Igor* function), as described above. The scattering needs to be computed for every streak hk (an adequate limited number of streaks and their multiplicity have been set up beforehand, depending on wavelength and 2θ range) for a series of l with a sufficiently small step width Δl. If Δl is too large, intensities for very sharp peaks, e.g. for large values of N_c and a regular polytype (α, β, γ or δ approaching zero or one), become overestimated or the peak centre may be missed. Empirically, a step width depending on N_c has been chosen: $\Delta l = 1/(8N_c(h+k+1))$. The computing time depends to a great extent on N_c, and increases with about N_c^2 for small N_c and N_c^3 for large N_c. In the refinement it has been constrained to stay below 500. Higher values of N_c would be indistinguishable anyway due to the limited resolution of the diffractometer used.

The scattered intensity as a function of l is then projected to the 2θ axis of a Debye–Scherrer diffractometer. At this stage we have the lattice constants, the wavelength and θ zero-shift as optionally refinable parameters. The resulting intensity is convoluted by a Lorentzian function to account for size broadening perpendicular to $\vec{c}$ (the size broadening parallel to $\vec{c}$ is already handled by the parameter N_c, the number of stacked layers). For anisotropic size broadening it is possible to use a very general phenomenological model, using the Scherrer formula, written as a linear combination of spherical harmonics (SPH).

$$\beta_{hkl} = \frac{\lambda}{D_{hkl}\cos\theta} = \frac{\lambda}{\cos\theta}\sum_{lmp} a_{lmp}\, y_{lmp}(\Theta_{hkl}, \Phi_{hkl}). \quad (9)$$

The values of y_{lmp} are given by Järvinen [30]. These normalized symmetrized real spherical harmonics up to the second order corresponding to the Laue class $\bar{3}m$ of ice Ic/Ih

polytypes are:

$$y_{00} = 1$$
$$y_{20} = \frac{3\cos^2\Theta - 1}{2}. \tag{10}$$

We have $\cos\Theta_{hkl} = \sqrt{l^2}/(c[l^2/c^2 + 4(h^2+kh+k^2)/3a^2]^{1/2})$ and the normalization condition that in direction $\vec{c}$ ($\Theta = 0$) the particle size is infinite (as already handled by N_c), which results in:

$$\beta_{hkl} = \frac{\lambda}{\cos\theta}\left(a_{00} + a_{20}\frac{3\cos^2\Theta_{hkl} - 1}{2}\right)$$
$$\beta_{00l} = \frac{\lambda}{\cos\theta}\left(a_{00} + a_{20}\frac{3\cos^2 0 - 1}{2}\right) = 0$$
$$a_{00} + a_{20}\frac{3-1}{2} = 0$$
$$a_{00} = -a_{20}$$
$$\beta_{hkl} = \frac{\lambda}{\cos\theta}\left(a_{00}\left(1 - \frac{3\cos 2\Theta_{hkl} - 1}{2}\right)\right) \tag{11}$$
$$\beta_{hkl} = \frac{\lambda}{\cos\theta}\left(a_{00}\left(\frac{2 - 3\cos 2\Theta_{hkl} - 1}{2}\right)\right)$$
$$\beta_{hkl} = \frac{\lambda}{\cos\theta}a_{00}\left(\frac{3 - 3\cos^2\Theta_{hkl}}{2}\right)$$
$$= \frac{\lambda}{\cos\theta}a_{00}\left(\frac{6c^2(h^2+kh+k^2)}{4(h^2+kh+k^2)c^2 + 3a^2l^2}\right)$$
$$\beta_{hk0} = \frac{\lambda}{\cos\theta}a_{00}\frac{3}{2}.$$

From this it follows that, for the characteristic size in the basal plane, $D_{hk0} = 2/(3a_{00})$.

The intensity modulation due to thermal motion is taken into account by a single isotropic overall Debye–Waller factor, which appears to be sufficient to fit the available powder diffraction data, which does not cover a very large Q-range.

Intensity is further modulated by the Lorentz factor L which has two components: the 'sample factor' accounts for the fraction of material in reflection orientation and is proportional to $(\sin\theta)^{-1}$ [31] and a geometrical factor accounting for the fact that not all the intensity in a diffraction cone is collected on the used diffractometer of Debye–Scherrer type:

$$L = \frac{1}{\sin\theta}\frac{\arcsin\frac{h_d/d_d}{\sin 2\theta}}{\pi}. \tag{12}$$

Here h_d/d_d is in a first approximation the ratio of detector height h_d to the sample–detector distance d_d. As the vertical focusing of the monochromator and the sample height are further non-negligible contributions, the value h/d has been refined from a reference powder pattern of hexagonal ice (at the end of the temperature program) to $h_d/d_d \approx 0.015$, but left fixed for further refinements as it shows a strong correlation with the scale factor. Compared to the closely related usual Lorentz factor definition, $L = (\sin\theta\sin 2\theta)^{-1}$ [31], the computed pattern corresponds better to the observation.

Finally, the result, scattering intensity as a function of 2θ, is convoluted depending on the diffraction angle 2θ with the experimental peak shape as a function of 2θ. These peak shapes have been extracted from a powder diffraction pattern of $Na_2Ca_3Al_2F_{14}$ [32] recorded under exactly the same setting in terms of instrument resolution and wavelength. This powder has proven to be extremely well crystallized, therefore, size and strain broadening effects can be neglected. The peak shape can be assumed to be determined exclusively from the diffractometer. Additionally, the cubic compound shows a high number of well-separated peaks over the whole range of 2θ. About ten peaks have been extracted manually, the shapes normalized to unity intensity. The shape at any 2θ is interpolated from the adjacent peak shapes.

4. Results

The model developed here can now be applied to measured diffraction data in a profile refinement procedure. Independently and simultaneously refined parameters are the scale factor of ice Ic, four factors of a polynomial expression describing the background, two lattice parameters a and c, the relative position of oxygen d in the direction of the fractional coordinate z and the relative position g of hydrogen on the connection line between neighbouring oxygen positions as used in the definition of structure factors in equation (6), an overall Debye–Waller factor for oxygen and hydrogen, the number of layers N_c, the four probabilities α, β, γ and δ and the parameter a_{00} after equation (11) inversely proportional to the size of the particles in the plane perpendicular to the stacking direction $\vec{c}$. In the region of coexistence of ice Ic with a precursor phase, up to eight further refinable parameters add to these 15 parameters. The refined data range from $2\theta = 20°$ to $2\theta = 145°$ and have been recorded at a wavelength of $\lambda = 2.4091$ Å. A first set of starting values for all parameters was obtained by trial, further on, in the sequential refinement of a series of evolving patterns in time and with temperature; the parameter set of the preceding or the following pattern in the series was taken therefore. There is some noteworthy correlation between scale and the Debye–Waller factor (0.7), the cubic and the square background term (0.8), N_c and the c-axis (0.7), δ and c (0.4), δ and N_c (0.6), α and β (0.5), α and γ (0.5), β and γ (0.5), and γ and δ (0.3). Nevertheless, the iterative refinement converges always and no parameter needs to be kept fixed. The curve fitting algorithm we used is the Levenberg–Marquardt nonlinear least-squares optimization algorithm [33] implemented in Igor Pro. The computing time for one full iterative refinement in Igor Pro ranges from about 6 min for $N_c = 70$ to about 80 min for $N_c = 500$ on an Apple MacBook Pro with 2.33 GHz Intel Core 2 Duo processor with 3 GB of memory. The reason, why the N_c^2 to N_c^3 dependence of the computing time for a single model becomes a roughly linear dependence on N_c is due to the fact that the refinement converges faster for higher N_c.

The model was used successfully to fit all data sets from the formation of ice Ic up to the onset of transformation of ice Ic into ice Ih at about 185 K. For ice Ic at 170 K we show the quality of the fit and the pair correlation probabilities $P_{AB\cdot AB}(m_3)$, $P_{AB\cdot BA}(m_3)$, $P_{AB\cdot BC}(m_3)$ and $P_{AB\cdot CA}(m_3)$ in figures 5 and 6. The clear differences in the diffraction patterns

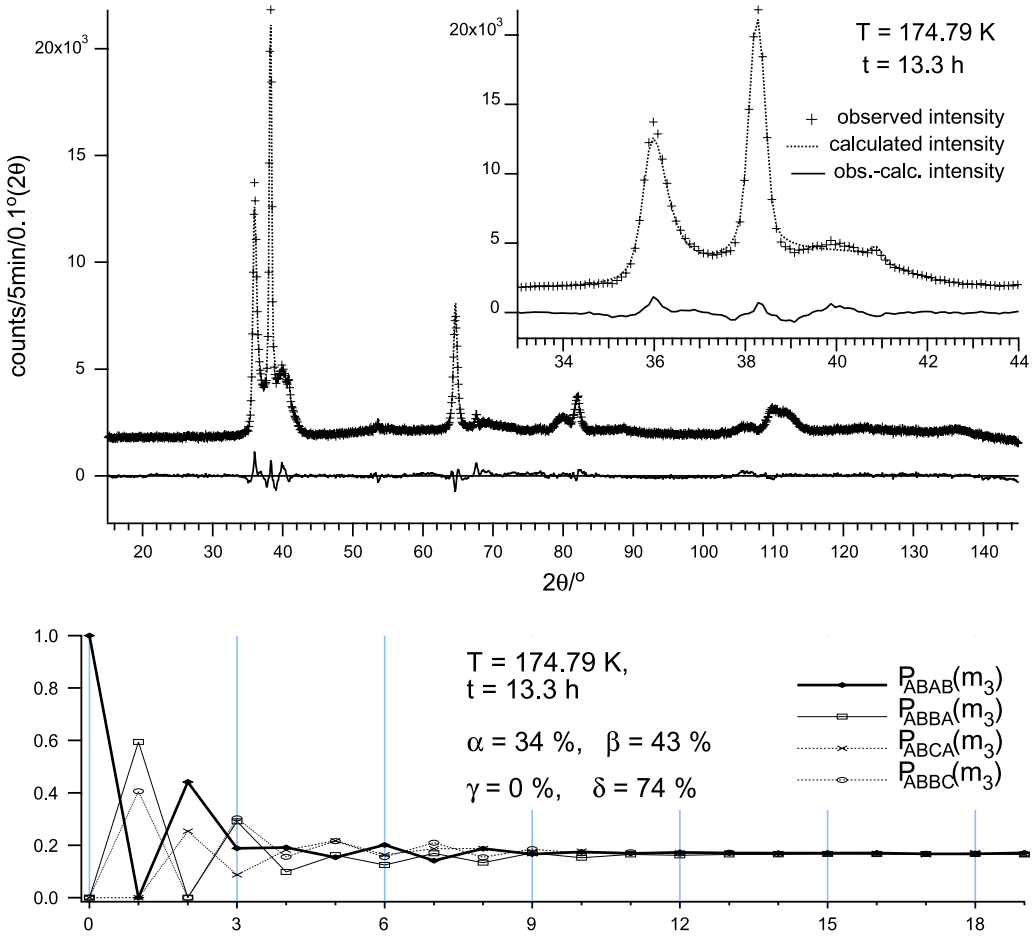

Figure 6. Diffraction pattern and fit of ice Ic from ice IX at the end of the 175 K stage after 13.3 h (top) and pair correlation probabilities in ice Ic at these conditions (bottom). A small contamination of ice Ih is visible and was present and stable from the beginning of the experiment.

of ice Ic from ice V and ice IX translate into differences in the stacking sequences.

Ice Ic from ice V has probabilities β and γ slightly below 40%, whereas δ is around 80% (thus the probability to have clusters of three cubic sequences or more is high) and α around 65% (thus two hexagonal sequences are normally enclosed in cubic sequences—which is the definition of a deformation fault in cubic packing). Cubic sequences are present in ice Ic from ice V to about 60%. The fact that pairs of two hexagonal sequences (w_{HH}) appear as often as each one of both probabilities to have pairs of cubic and hexagonal stacking sequences in either order (w_{HK} and w_{KH}) to about 20% means again that hexagonal sequences always appear in pairs (deformation faults), nearly never as a single hexagonal sequence (growth faults) and nearly never in clusters of more than two hexagonal sequences.

Ice Ic looks rather different from ice IX: γ is close to zero, which means that single hexagonal sequences are forbidden, α is much lower and reaches about 40% at 175 K. δ is, as in the case of ice Ic from ice V, higher than α, whereas β decreases over time to about 40% at 175 K. The concentration of cubic sequences is about 42% at 175 K. This form of ice is slightly less rich in interfaces between the cubic and the hexagonal stacking rule than ice Ic from ice V, with w_{HK} of about 15%.

It is interesting to note that the crystallite size parallel to $\vec{c}$, $D_{00l} = N_{\mathrm{c}} \cdot c$, and perpendicular to $\vec{c}$, $D_{hk0} = 2/3 \cdot a_{00}$, following equations (9) and (11) is basically the same. Crystals are thus isometric, neither platelet, nor needle shaped. The temperature dependency of the particle size and changes in the stacking sequences will be discussed in the accompanying paper [20]. Here we only demonstrate that the model provides a very good fit to the diffraction data and allows for the first time a full-pattern least-squares analysis of the diffraction data of ice Ic. It should be noted, however, that the possibility to follow the temperature-induced changes in the defect structure by fitting an appropriate set of parameters provides additional support for the sound physical basis of the model.

5. Discussion

The stacking-fault model described in section 3 allows a very satisfactory profile fitting of all powder diffraction data of ice Ic obtained from ice V as well as ice IX for the whole temperature range investigated [20]. As expected from the different appearance of the diffraction pattern, the stacking sequences are found to be significantly different for the two cubic ices of different origin. For the first time, these differences can now be quantified in terms of probabilities of stacking

polytypes and (anisotropic) crystallite size and followed as temperature-induced changes take place. This seems far more satisfactory than earlier attempts to fit with *ad hoc* assumptions the complex powder pattern of ice Ic. One such assumption was the presence of small amounts of low-density amorphous ice suggested by Elarby-Aouizerat *et al* [12] in an attempt to describe the powder pattern of ice Ic precipitated from a glassy $LiCl \cdot H_2O$ matrix; the excess intensity found in their peak fitting approach centred at $Q \approx 1.7$ Å^{-1} (i.e. between the cubic 111 and the hexagonal 101 peak) turned out to be perfectly well described by our stacking-fault model. Elarby-Aouizerat *et al* [12] also suggested the existence of a Warren-type profile of the leading hexagonal 100 reflection originating in the presence of laterally randomly oriented sheets. Again, our anisotropically broadened one-dimensional stacking-fault model describes this part of the powder pattern fully satisfactorily without such a complication. Of course, we cannot exclude a small amount of lateral disorder in the stacking sequences, but given the rather directional H-bond forces between the sheets we do not expect large lateral displacements in crystalline ice. Thus we are convinced that our model is not only simpler but also builds on more realistic physical assumptions.

6. Summary and outlook

A structural model for the description of ice Ic is proposed and applied to neutron diffraction data. Ice Ic contains a considerable level of hexagonal stacking sequences, preferably occurring in pairs of two subsequent hexagonal stacking sequences (deformation faults, as suggested by Kuhs *et al* [2]). The crystallites of ice Ic obtained from relaxation of ice V and ice IX are small, containing around 130 stacking sequences (about 500 Å in $\vec{c}$-direction) at 175 K. After all, this so-called 'cubic ice' is not really cubic, but trigonal at most (space group $P3m1$).

The presented computing method is revealed to be satisfactory for a quantitative description of ice Ic from powder diffraction data. It allowed us, for the first time, to fit the observed powder diffraction patterns of ice Ic to a structural model. The main result thus is that indeed ice Ic is a regular stacking-faulted phase with small crystallites, and the model describes fully the nature of this phase, which had remained obscure since its first discovery more than 64 years ago [1].

Still, a word of caution is in order: as is general in a multi-dimensional parameter space, a least-squares method does not guarantee that we can obtain the best possible model, i.e. the correct set of probabilities α, β, γ and δ. An optimization method, such as simulated annealing should be invoked in order to lead to the best solution, which can further be refined with the least-squares method. Nevertheless, the smoothness of the least-squares convergence and the only moderate correlations amongst the stacking-fault parameters give us confidence in the obtained results.

Instead of a sharply peaked distribution of the stacking-faulted phase to be described with one set of α, β, γ and δ, N_c and other parameters, a broader and even skewed distribution should be considered. It has to be checked whether there is a solution to describe such a distribution without the cumbersome computing for many different phases which have to be combined for describing such a distribution.

The computing has been performed inside the commercially available Igor Pro software [28], invoking fast, so-called *XOP*s [29] (externally subroutines programmed entirely in C). The code should be translated totally to a programming language like C in order to become more efficient. Further on, the code should be generalized to be able to handle similar problems of one-dimensional stacking disorder in other crystalline materials and thus become possibly an alternative to DIFFaX [34] (which does not permit refinements) and FAULTS [35] (based on DIFFaX but permitting refinement of parameters).

Acknowledgments

The authors thank the ILL for allocated neutron beam time (28th–30th May 2007) and technical support on the instrument D20 in the frame of the proposal 5-24-271. We are grateful to Eberhard Hensel and Andrzej Falenty from the Universität Göttingen for the technical support during the sample preparation and the Deutsche Forschungsgemeinschaft (DFG) for financial support via the grant Ku-920/11 in the framework of its programme 'Mars and Earth-like planets'.

References

[1] König H 1943 Eine kubische Eismodifikation *Z. Kristallogr.* **105** 279–86
[2] Kuhs W F, Bliss D V and Finney J L 1987 High-resolution neutron powder diffraction study of ice I_c *J. Physique* C1 **48** 631–6
[3] Lisgarten N D and Blackman M 1956 Cubic form of ice *Nature* **178** 39–40
[4] Shallcross F V and Carpenter G B 1957 X-ray diffraction study of the cubic phase of ice *J. Chem. Phys.* **26** 782–4
[5] Dowell L G and Rinfret A P 1960 Low-temperature forms of ice as studied by x-ray diffraction *Nature* **188** 1144–8
[6] Bertie J E and Jacobs S M 1977 Far-infrared absorption by ices Ih and Ic at 4.3 K and the powder diffraction pattern of ice Ic *J. Chem. Phys.* **67** 2445–8
[7] Klotz S, Besson J M, Hamel G, Nelmes R J, Loveday J S and Marshall W G 1999 Metastable ice VII at low temperature and ambient pressure *Nature* **398** 681–4
[8] Klug D D, Paul Handa Y, Tse J S and Whalley E 1989 Transformation of Ice VIII to amorphous ice by melting at low temperature *J. Chem. Phys.* **90** 2390–2
[9] Mayer E and Hallbrucker A 1987 Cubic ice from liquid water *Nature* **325** 601–2
[10] Kohl I, Mayer E and Hallbrucker A 2000 the glassy water–cubic ice system: a comparative study by x-ray diffraction and differential scanning calorimetry *Phys. Chem. Chem. Phys.* **2** 1579–86
[11] Arnold G P, Finch E D, Rabideau S W and Wenzel R G 1968 Neutron-diffraction study of ice polymorphs. III. Ice Ic *J. Chem. Phys.* **49** 4354–69
[12] Elarby-Aouizerat A, Jal J F, Dupuy J, Schildberg H and Chieux P 1987 Comments on the ice I_c structure and I_c to I_h phase transformation mechanism: a neutron scattering investigation of ice precipitates in glassy $LiCl{\cdot}D_2O$ *J. Physique* C1 **48** 465–70
[13] Steytler D C, Dore J C and Wright C J 1983 Neutron-diffraction study of cubic ice nucleation in a porous silica network *J. Phys. Chem.* **87** 2458–9

[14] Paterson M S 1952 X-ray diffraction by face-centered cubic crystals with deformation faults *J. Appl. Phys.* **23** 805–11
[15] Londono J D 1989 *PhD Thesis* University of London
[16] Kuhs W F, Londono D, Mayer E, Hallbrucker A and Finney J L 1989 Neutron powder diffraction studies on the formation and stability of Ice Ic *Z. Kristallogr.* **186** 174–5
[17] Hansen T C, Falenty A and Kuhs W F 2007 Modelling ice Ic of different origin and stacking-faulted hexagonal ice using neutron powder diffraction data *Special Publication* vol 311 *Physics and Chemistry of Ice* ed W F Kuhs (Cambridge: Royal Society of Chemistry) pp 201–8
[18] Weiss Z and Capkova P 1999 Effect of stacking disorder on the profile of the powder diffraction line *IUCr Monographs on Crystallography* vol 10 *Defect and Microstructure Analysis by Diffraction* ed R L Snyder, J Fiala and H J Bunge (New York: Oxford University Press) pp 318–29
[19] Berliner R and Werner S A 1986 Effect of stacking faults on diffraction: the structure of lithium metal *Phys. Rev.* B **34** 3586–603
[20] Hansen T C, Koza M M, Lindner P and Kuhs W F 2008 Formation and annealing of cubic ice. II. Kinetik study *J. Phys.: Condens. Matter* **20** 285105
[21] Wilson A J C 1941 Imperfections in the structure of cobalt II. Mathematical treatment of proposed structure *Proc. R. Soc.* A **180** 277–85
[22] Guinier A 1963 *X-Ray Diffraction* (San Francisco, CA: Freeman)
[23] Jagodzinski H 1949 Eindimensionale Fehlordnung in Kristallen und ihr Einfluss auf die Röntgeninterferenzen. 1. Berechnung des Fehlordnungsgrades aus den Röntgenintensitäten *Acta Crystallogr.* **2** 201–7
[24] Hendricks S and Teller E 1942 *J. Chem. Phys.* **10** 147
[25] Ellinger F H and Zachariasen W H 1953 The crystal structure of samarium metal and of samarium monoxide *J. Am. Chem. Soc.* **75** 5650–2
[26] Danne A H, Rundle R E, Smith H G and Spedding F H 1954 *Acta Crystallogr.* **7** 532
[27] Ramsdell L S 1947 Studies on silicon carbide *Am. Mineral.* **32** 64–82
[28] 2007 *Igor Pro Version 6.0* Wavemetrics Inc., Lake Oswego, Oregon, USA
[29] 2006 *Igor XOP Toolkit Version 5* Wavemetrics Inc., Lake Oswego, Oregon, USA
[30] Järvinen M 1998 Application of symmetrized harmonics expansion to correction of the preferred orientation effect *J. Appl. Crystallogr.* **26** 525–31
[31] van Laar B and Yelon W B 1984 The peak in neutron powder diffraction *J. Appl. Crystallogr.* **17** 47–54
[32] Courbion G and Ferey G 1988 $Na_2Ca_3Al_2F_{14}$: a new example of a structure with 'independent F^-'—a new method of comparison between fluorides and oxides of different formula *J. Solid State Chem.* **76** 426–31
[33] Press W H, Flannery B P, Teukolsky S A and Vetterling W T 1992 Numerical recipes in C *Numerical Recipes in C* 2nd edn (New York: Cambridge University Press) p 994
[34] Treacy M M J, Newsam J M and Deem M W 1991 A general recursion method for calculating diffracted intensities from crystals containing planar faults *Proc. R. Soc.* A **433** 499–520
[35] Casas-Cabanas M, Rodriguez-Carvajal J and Palacin M R 2006 FAULTS, a new program for refinement of powder diffraction patterns from layered structures *Z. Kristallogr.* Suppl. 23 243–8